Liversidge Research Lecture
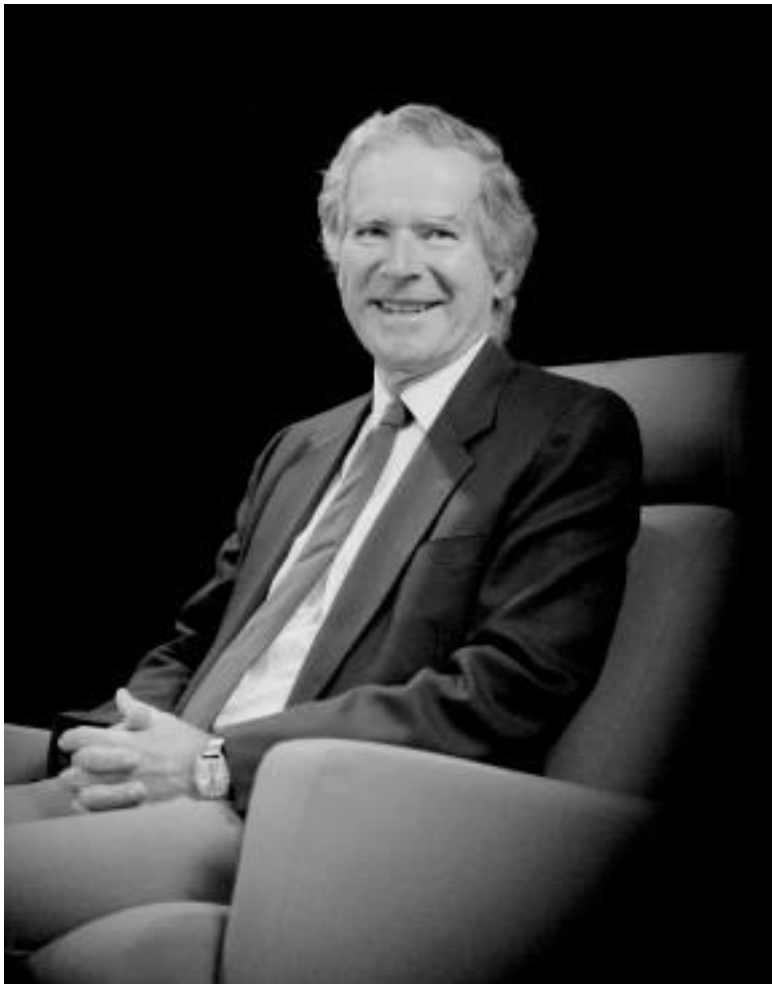
No. 20
1976

COORDINATION, TOPOLOGY AND STRUCTURE IN TRANSITION METAL OXIDES

RAYMOND L. MARTIN

The Royal Society of New South Wales

Raymond Leslie Martin

Liversidge Research Lecturer No. 20, 1976.

RAYMOND LESLIE MARTIN 1926 -

Raymond Leslie Martin was born in Melbourne on 3 February 1926.   His secondary education was at Scotch College, Melbourne (1932-1941), then at North Sydney Boys High School (1942).   He graduated B.Sc. at the University of Melbourne in 1945, and M.Sc. (supervisor, J.S. Anderson, later Professor, and FRS) in 1947, then for the period 1947-1949 he was Senior Demonstrator in the Chemistry Department, and Senior Tutor at Queen's College, University of Melbourne.   In 1949, with an 1851 Exhibition Overseas Scholarship he went to Cambridge University, where he worked with Professor H.J. Emeléus, FRS on coordination compounds of boron trifluoride, and graduated Ph.D. in 1951.   Then for the period 1952-1954 he was an 1851 Senior Scholar and Research Fellow at Sidney Sussex College, Cambridge.   In 1954 he returned to Australia as Senior Lecturer at the University of Technology, Sydney (later the University of N.S.W.) until 1959, when he took the position of Section Leader, Physical and Inorganic Chemistry, Central Research Laboratory, ICI (ANZ) in Melbourne.   In 1962 he was appointed as the Foundation Professor and Head of the Department of Inorganic Chemistry, University of Melbourne, which position he held until 1972.   During that time he spent periods of leave as Visiting Scientist, Bell Telephone Labs., Murray Hill, New Jersey (1967), and Visiting Professor at Colombia University, New York, USA (1972). In 1971 he was Dean, Faculty of Science, and Acting Dean, Faculty of Music at the University of Melbourne.

In 1972 he was appointed the Foundation Professor of Inorganic Chemistry at the Research School of Chemistry, Australian National University, acting as Dean for the period 1976-1977. In 1977 he was appointed as Vice-Chancellor and Professor at Monash University, Melbourne, which position he held for ten years, then was Professor of Chemistry at Monash University from 1987 until he retired in 1991. His research interests have been mainly in magnetochemistry, coordination chemistry, and chemistry of the solid state. During 1968-1969 he was President of the Royal Australian Chemical Institute (RACI); for the period 1988-1992 he was Chairman of the Australian Science and Technology Council (ASTEC), and between 1989-1992 was a Member of the Prime Minister's Science Council (PMSC) and the Government's Coordination Committee on Science and Technology (CCST).

In the 1980s and 1990s Ray Martin acted in various capacities in numerous institutional and national boards and committees in the Arts, Sciences, Business and philanthropic organizations.   He holds Emeritus Professorships at both the Australian National University (1977-) and Monash University (1991-).

Honours and Awards (Pre-2014)

1945   Fred Walker Prize and *proxime accessit* Dixon Prize in the final year Chemistry, University of Melbourne

1956   FRACI (Fellow of the Royal Australian Chemical Institute)

1968   H.G. Smith Medal, RACI

1968   Sc.D., Cambridge University, UK

1971   FAA

1974   FRSC (Fellow of the Royal Society of Chemistry)

1975   Archibald D. Ollé Prize, RACI

1976   Liversidge Research Lecture, Royal Society of New South Wales

1977   Queen's Silver Jubilee Medal

1978   G.J. Burrows Medal, RACI

1978   D.Sc., Australian National University

1987   Officer Order of Australia (AO)

1989   A.E. Leighton Medal, RACI

1989   FTSE (Fellow of the Australian Academy of Technological Sciences and Engineering).

1992   L.L.D., *honoris causa*, Monash University

1995   D.Sc., *honoris causa*, University of Melbourne

2001   FAIM (Fellow of the Australian Institute of Management)

Biographical Source

Personal communication.

Scientific Publications by R.L. Martin

Between 1950 and 1999 R.L. Martin had some 176 publications on inorganic chemistry, including authorship/co-authorship of 3 book chapters.

COORDINATION, TOPOLOGY AND STRUCTURE IN TRANSITION METAL OXIDES*

RAYMOND L. MARTIN

Research School of Chemistry, The Australian National University, Canberra

ABSTRACT.   The role of defects in the real structure of transition metal oxides which exhibit gross departures from simple stoicheiometries† is reviewed.   The classical notion of a randomized distribution of non-interacting point defects is no longer tenable being replaced by the emerging recognition that a high level of organization into discrete clusters or more extended assemblies of defects is an inherent feature of the real structure of defect solids.   The concept of octahedral coordination of vacant oxygen sites, taken in conjunction with topological analysis, is shown to contribute considerable insight into the transformational and structural relationships between defect oxides of the fluorite type.

Introduction

It is a distinction indeed to be invited by the Royal Society of New South Wales to be their Liversidge Research Lecturer.   The Lectureship honours Professor Archibald Liversidge who profoundly influenced the development of science in Australia.   During a career of remarkable distinction he was appointed to the Chair of Chemistry and Mineralogy in Sydney at the age of 24 and was elected to the Fellowship of the Royal Society (London) at 34.   He founded the Australasian Association for the Advancement of Science, the Faculty of Science, and the School of Mines in the University of Sydney and was the driving force behind the advancement of the Royal Society of New South Wales for many decades.

The field which I wish to evaluate this evening, structural inorganic chemistry of the solid state, has its origins in mineralogy.   This is an appropriate association because Liversidge, as Professor of Chemistry and Mineralogy, brought together the greater part of the non-Australian mineral and geological collection at the Australian Museum in Sydney and published a significant survey of the minerals of New South Wales in 1888.

All crystalline solids contain imperfections.   Semi-conduction, thermo-electric effect and transistor technology provide familiar examples of electronic properties which have their origin in deviations from perfect crystalline order.   Oxides of the transition metals range from those which deviate from ideal stoicheiometric composition by an amount which is imperceptible chemically to those where departures from stoicheiometry are gross.   Reduction in miniscule of TiO_2 yields $TiO_{1.9986}$ where the concentration of point defects could hardly exceed 10^{-4} (Bursill *et al.,* 1970); reduction in majuscule of CeO_2

----

yields the sesquioxide $CeO_{1.5}$ where 25% of the anion lattice sites become untenanted. Any theoretical analysis of thermodynamic equilibrium, transport and diffusion, reactivity, electronic and other properties of solids can only be based on an understanding of the structural role of defects and the nature of their interactions.

In this lecture attention will be directed to non-stoicheiometric oxides which possess structures either of the rock salt (NaCl) or the fluorite (CaF_2) type with emphasis on the means by which quite high concentrations of point defects are assimilated by the host lattice. If one considers a regular two-dimensional array with imperfections (*e.g.*, vacant lattice sites in Fig. 1), the essential problem is to ascertain whether these are distributed randomly or are correlated in position.
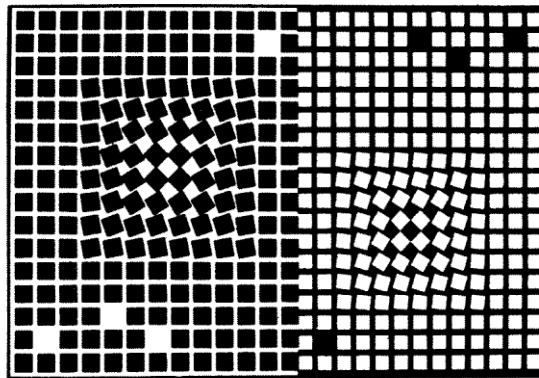

FIGURE l. Point defects (vacant sites) introduced into ordered two-dimensional lattice array (with apologies to Victor Vasarely).

Random *versus* Ordered Defects

At extremely low concentrations of point defects, the classical model (Schottky and Wagner, 1930) assumes that interactions between them are absent so that their distribution is random and the change in configurational entropy of the crystal is that for ideal mixing of the defects. However, as the concentration of randomized point defects becomes higher, an increasing proportion of defects will move into juxtaposition so that the structural and thermodynamic implications can no longer be ignored. In a real crystal, interactions between point defects is present and the tendency for them to become ordered has important structural consequences (Bursill *et al.*, 1970). The traditional notion of randomized point defects as a basis for explaining gross departures from simple stoicheiometry must be abandoned and replaced by the concept of "correlated defects" as intrinsic structure-determining elements of the defective solid.

Ordering of Defects: Superstructure and Coherent Intergrowth

The structural consequences of correlation between interacting defects is exemplified by the monoxides of first-row transition metals (*e.g.*, Ti, V and Fe) which are derived from the rock salt structure. Although existence of the non-stoicheiometric ™-phase ($TiO_{0.7}$ - $TiO_{1.25}$) has been recognized since 1939, evidence for the nature of the real defect structure of titanium oxides in this composition region was forthcoming only after a combined attack by the methods of electron microscopy, electron and X-ray diffraction

some thirty years later (Watanabe *et al.,* 1970).   Below 1000˚C there are two distinct ordered phases at composition $TiO_{1.00}$ and $TiO_{l.25}$, the structures of both being super-lattices based upon the rock salt type, with every occupied lattice site assignable to a site of the parent structure (Fig. 2a).   Surprisingly, the "stoicheiometric" phase $TiO_{1.00}$ is grossly non-stoicheiometric, the interpenetrating face-centred cubic (f.c.c.) arrays of titanium and oxygen having one-sixth of each type of atom formally missing, *i.e.,* $Ti_{5/6}O_{5/6}$.   The vacant cation and anion sites are octahedrally coordinated by oxygen and titanium atoms respectively, the octahedra sharing *trans*-apices to yield extended strings of composition $\square_{Ti}O_5$ and $\square_OTi_5$ (Fig.2b).   In the oxygen-rich $TiO_{l.25}$, the high concentration of defects (~20%) is confined solely to the cation sub-lattice, *i.e.,* $Ti_{4/5}O$. The structure is composed of extended $\square_{Ti}O_5$ strings blended with four titanium atoms giving the observed composition (Fig.2a).   Interactions of point defects in both phases have led to the development of extended regions of long-range order, *i.e.,* the generation of a super-lattice of the rock salt structure.

There is a close relationship between the structural elements of the $TiO_{1.00}$ and $TiO_{l.25}$ phases which make them dimensionally compatible so that intergrowth between them can occur coherently at a common, defect-free $(120)_{cub}$ planar interface (Fig. 2a). For oxides with compositions intermediate between $TiO_{1.00}$ and $TiO_{l.25}$, prolonged annealing generates lamellae comprised of alternate thin layers of the two boundary phases in the appropriate proportions.
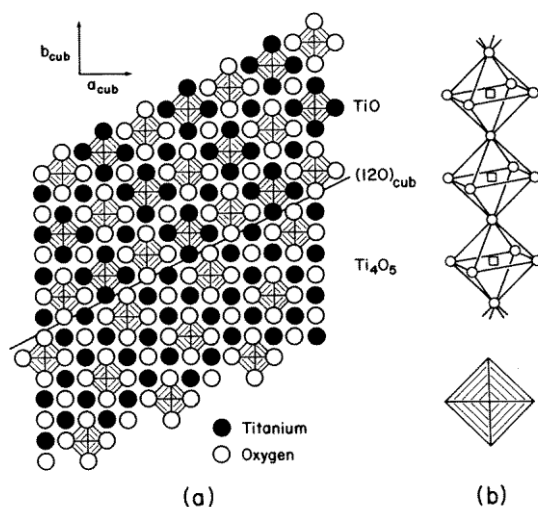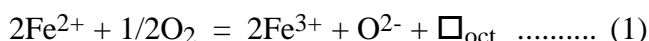

FIGURE 2. (a) The idealized structures of ordered TiO and Ti_4O_5 coherently intergrown across a $(120)_{cub}$ plane of rock salt structure; (b) Vacant cation and anion sites are octahedrally coordinated by oxygen and metal atoms respectively, and occur as extended strings of composition $\square_MO_5$ and $\square_OM_5$ to yield $Ti_{5/6}O_{5/6}$.

Although the point defects are located at lattice sites of the parent rock salt structure, they are ordered geometrically so that the repeat unit of the new structure is larger than that of the parent and of lower symmetry.   In a formal sense, the binary phases $TiO_{1.00}$ and $TiO_{1.25}$ can be regarded as a ternary system (anion, cation, defect), the defect being incorporated as the third component of the superstructure.
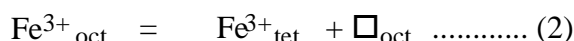
Ordering of Defects: Clusters

In the case of FeO, interactions between defects promote their organization into complex groups of correlated defects.   This aggregate of defects or "cluster" becomes the new structural entity on which periodicity in the superstructure is based.

Ferrous oxide (rock salt type structure) is thermodynamically stable only above 570˚C.   Under ambient conditions the f.c.c. oxygen sub-lattice remains essentially complete but the cation sublattice is deficient of iron in the range $Fe_{0.85}O$ - $Fe_{0.95}O$. To maintain electrical neutrality in the defect oxide, there are necessarily two Fe^{3+} ions for each vacant cation site,

$$2Fe^{2+} + 1/2O_2 \;=\; 2Fe^{3+} + O^{2-} + \square_{oct} \;\; .... \;\; (1)$$

Since the ligand field stabilization of energy of Fe^{3+} (high-spin $3d^5$) in an oxygen lattice is zero, it has no preference for substitutional (octahedral) as opposed to interstitial (tetrahedral) sites.   Indeed, magnetic neutron scattering and X-ray crystallographic studies establish that a substantial fraction of Fe^{3+} cations migrate to tetrahedral interstitial sites (Koch *et al.*, 1969),

$$Fe^{3+}_{oct} \;\;=\;\; Fe^{3+}_{tet} \;+\; \square_{oct} \;\; .... \;\; (2)$$

The two types of point defect, $\square_{oct}$ and Fe^{3+}_{tet} , interact strongly and coalesce to form a defect cluster comprising four tetrahedrally coordinated iron(III) atoms and thirteen octahedral vacant cation sites (Fig. 3).   The $\{(Fe_4 \square) \square_{12}\}$ clusters being dimensionally compatible, can intergrow coherently with defect-free regions of the host rock salt structure. The structure of the cluster is much more complex than a simple aggregation of
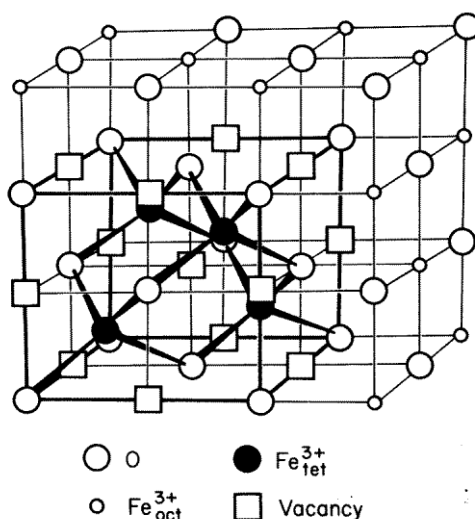

FIGURE 3. Fe_{1-x}. Koch-Cohen cluster comprising four tetrahedral iron atoms surrounded by thirteen vacant sites in rock salt structure.

cation vacancies.   It arises from both an aggregation process and a local modification of the rock salt matrix, and represents, indeed, the complete transformation of the contents of one unit cell of NaCl structure into one unit cell of zinc blende (ZnS) structure which is dimensionally compatible, both having f.c.c. anion lattices (Fig. 4).
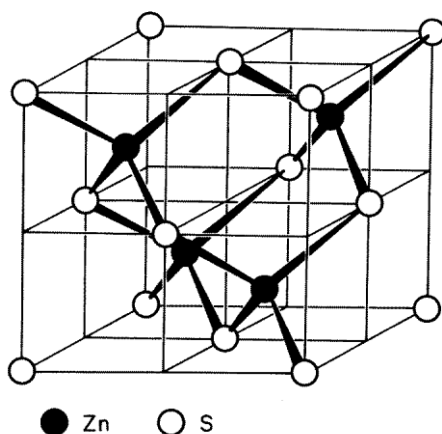
● Zn   ○ S

FIGURE 4.   Zinc blende structure.

The clusters themselves tend to order under coulombic forces to develop a superstructure. The composition and configuration of this defect cluster is reminiscent of the polynuclear coordination compound, basic zinc(II) acetate, $\{Zn_4O(CH_3CO_2)_6\}$ (Koyama et al. 1954).

Defect Elimination: Crystallographic Shear

The early transition metals in higher oxidation states (Ti^{4+}, V^{4+}, Nb^{5+}, Mo^{6+}, and W^{6+}) preserve octahedral coordination of the central metal ion in their binary oxides. Even though reduction of the metal to a lower oxidation state involves the removal of oxygen from the parent lattice, unlike rock salt and fluorite-type oxides, vacant anion sites are not retained in the non-stoicheiometric phase.   Rather, the stoicheiometric change is accommodated by the elimination from the crystal of a complete plane of anion sites followed by a formal structural operation, crystallographic shear (CS), which restores octahedral coordination about the metal ion (Anderson et al., 1967).   There is a concomitant increase from two to three in the number of metal atoms coordinated to
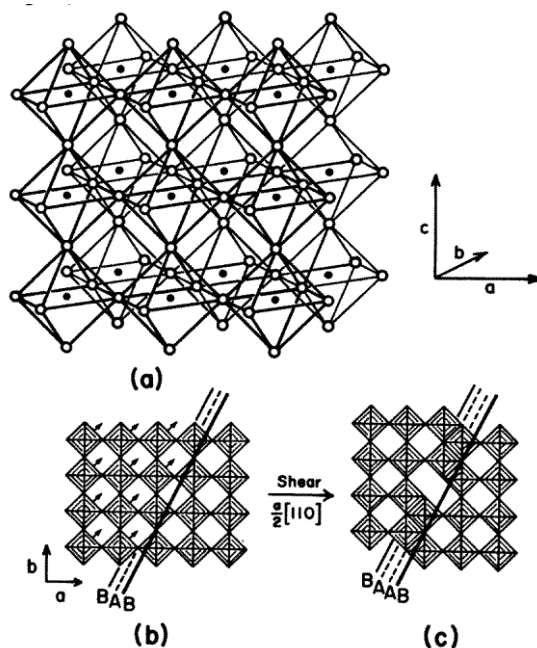

FIGURE 5.   (a) ReO_3 structure type;   (b) ReO_3 represented as apex-sharing ReO_6 octahedra and projected on the (011) plane; (c) formation of CS plane which occurs in Mo_8O_{23}.

certain oxygen atoms. For example, the regular elimination of the CS plane (120) of oxygen atoms in MoO_3 (ReO_3 structure type; Fig. 5a) generates the non-stoicheiometric oxide Mo_8O_{23}, the first member of the homologous series of ordered oxides M_nO_{3n-1} where $8 \leq n \leq 12$ (Fig.5c). In the MoO_3 parent (Fig. 5b), the sequence of planes parallel to (120) is

$$\cdots\cdot ABABAB \cdot\cdots$$

($A = MoO_2$; $B = O$). The regular removal of every nth B-plane of oxygen atoms from the parent structure yields the homologue of generic formula $(MoO_2)_nO_{n-1}$; ie., M_nO_{3n-1} (Fig.5c). The elimination of anion vacancies by crystallographic shear is also common in ordered phases based on the rutile (TiO_2) structure (cf. Table 1).

TABLE 1

Crystallographic Shear in the ReO_3 and TiO_2 Structures*

Parent Structure	Orientation of CS Plane	Series Formula	n	Examples
ReO_3	(100)	M_nO_{3n-1}	2	$R-Nb_2O_5$
			3	Nb_3O_7F
	(130)	M_nO_{3n-2}	20, etc.	$W_{20}O_{58}$,etc.
	(120)	M_nO_{3n-1}	$8 \leq n \leq 12$	Mo_8O_{23}
Rutile	(121)	M_nO_{2n-1}	$4 \leq n \leq 9$	$Ti_4O_7 - Ti_9O_{17}$
				$V_4O_7 - V_9O_{17}$
	(132)	M_nO2_{n-1}	$16 \leq n \leq 36$	$Ti_{16}O_{31} - Ti_{36}O_{71}$

*After Anderson (1974).

Non-Stoicheiometric Oxides of Fluorite Type

In the terms of his bequest, Liversidge specified that emphasis "shall be upon recent researches and discoveries ....". Accordingly, I will now discuss some new concepts concerning the nature of defect solids of the fluorite type.

A distinguishing feature of the oxides of the early transition metals in high oxidation states, (Ti^{4+}, V^{5+}, Nb^{5+}, Ta^{5+}, Mo^{6+}, W^{6+}) discussed earlier, is that the MO_6 coordination polyhedron remains intact in oxides which depart from a simple stoicheiometry. The oxygen lattice remains invariant in these phases and deviations in composition from the elementary MO_2 or MO_3 stoicheiometry are brought about by peripheral corner- or edge-sharing of the MO_6 octahedra. As we have seen, this enables the structure of compounds with complex compositions to be illustrated with precision in two dimensions by employing the conventional projections of an idealized MO_6 octahedron (Fig. 5). Indeed, in favourable circumstances, the metal-centred octahedra are revealed directly by lattice imaging techniques in the electron microscope (Allpress, 1969) and this has produced new and deep insights into the real structure of the non-stoicheiometric oxides of the early transition metals (Allpress et al., 1969).

A parallel development in the depth of our understanding of the nature of the defect oxides of the lanthanide and actinide elements and some of the larger transition metals (e.g. Hf^{4+}, Zr^{4+}) has not been forthcoming. There are a number of reasons why their structural characterization has remained elusive. Oxygen can be transferred with extraordinary ease between the MO_x lattice and the ambient gas phase, even at relatively low temperatures (200-300˚C) so that the synthesis of well-ordered crystals is inherently difficult (the remarkably high oxygen mobility inhibits the quenching-in of both composition and crystallographic order in samples equilibrated at even moderate temperatures. Of course, it is just this feature which leads to the hopeful expectation that fluorite-type oxides can be developed into successful refractory electrodes for fuel cells and other technological uses. Although very small crystals of non-stoicheiometric praseodymium oxides have been grown by hydrothermal techniques, problems of crystallographic twinning, coherent intergrowth between homologous phases, absorption errors and large superstructures of low symmetry have all combined to make studies, even with single crystals, a formidable task.

The technique of lattice imaging, which has proved to be so incisive for CS structures which involve interstitial heavy metal atoms, does not produce the same marked contrast in images of the fluorite oxides. However, in the case of $Tb_{11}O_{20}$ periodicities imposed on the structure by oxygen vacancies appear to have been discerned in the bright field image (Kunzmann *et al.,* 1975). The vacancies are not imaged directly but the periodicity which they impose on the potential field may be discerned in the image.

Because of these difficulties, current efforts are being directed towards the neutron profile technique and the determination of superstructure lattice parameters from electron diffraction patterns taken in a high resolution transmission electron microscope from very small single crystals (average size; 1μm). This enables the unit cell dimensions and

TABLE 2
Some Ordered Fluorite Type Oxides

Composition	Binary Oxides	Ternary Oxides
$M_{2.00}$	$CeO_2,PrO_2,TbO_2, HfO_2,ThO_2,PaO_2,$ $UO_2,NpO_2,PuO_2,AmO_2,CmO_2,BkO_2$	
$MO_{1.857}$		©-$Zr_{10}Sc_4O_{26}$
$MO_{1.833}$	®-$Pr_{12}O_{22}$	
$MO_{1.818}$	$Ce_{11}O_{20}$, ™-$Pr_{11}O_{20}$, $Tb_{11}O_{20}$	
$MO_{1.800}$	$Ce_{10}O_{18}$, Σ-$Pr_{10}O_{18}$	ʻ1-$CaHf_4O_9$
$MO_{1.778}$	Ce_9O_{16}, ʼ-Pr_9O_{16}	ʻ-$Ca_2Hf_7O_{16}$
$MO_{1.760}$		ʻ2-$Ca_6Hf_{19}O_{44}$
$MO_{1.750}$		pyrochlore, $La_2Ti_2O_7$, $Gd_2Zr_2O_7$
$MO_{1.714}$	Ce_7O_{12}, ǀ-Pr_7O_{12},Tb_7O_{12} $Zr_3Yb_4O_{12}$	UY_6O_{12}, $Zr_3Sc_4O_{12}$,
$MO_{1.667}$	ǀ-Pr_6O_{10}	Sr_2UO_5, Cd_2UO_5
$MO_{1.600}$		
$MO_{1.50}$	Y_2O_3, Pr_2O_3, Sb_2O_3, ®-Bi_2O_3, bixbyite(⟨-Mn_2O_3), In_2O_3, Te_2O_3	

possible space groups of the intermediate phases as well as the transformation matrices to be defined in terms of the fluorite sub-structure. In defect oxides of the fluorite structure type (Table 2), the non-stoicheiometry is accommodated on untenanted anion sites, the cation sub-lattice remaining essentially intact. The central problem is to ascertain the superstructural pattern which reflects the ordering of anion vacancies in order that underlying structural principles may be defined. Unfortunately, the coordination sphere of the metal atom in dioxides such as CeO_2, HfO_2 and UO_2 is comprised of a cube of oxygen anions which precludes two-dimensional projection of MO_6 octahedra along 2-, 3- and 4-fold axes which have proved to be so illuminating for TiO_2 or ReO_3 based structures. Attempts to represent the fluorite structure by the edge-sharing of MO_8 polyhedra are cumbersome (Fig. 6) and provide only limited insight into the distribution of vacancies in oxides which deviate from elementary MO_2 composition (Sawyer *et al.*, 1965).

In an attempt to circumvent this problem, we can depart from our conventional metal-centred frame of reference and contemplate the fluorite lattice in terms of its
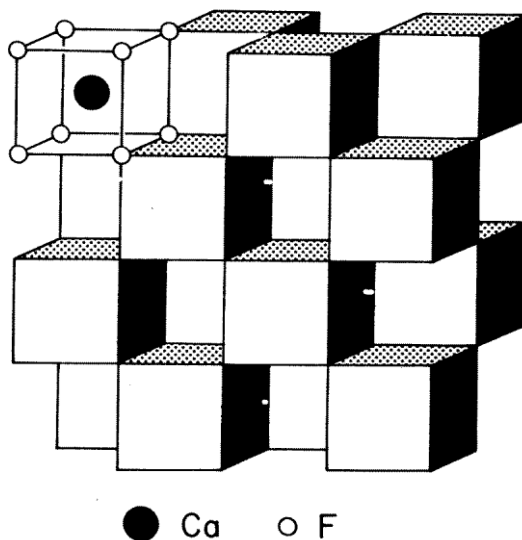

● Ca   ○ F

FIGURE 6. Fluorite structure represented as edge-sharing MO_8 cubes.

anion-centred polyhedra (Martin, 1974). Examination of the MO_2 structure reveals that each oxide anion is coordinated tetrahedrally by four cations to form an octant of the fluorite cube with the composition $M_{0.5}O$. Eight such octants arranged in juxtaposition
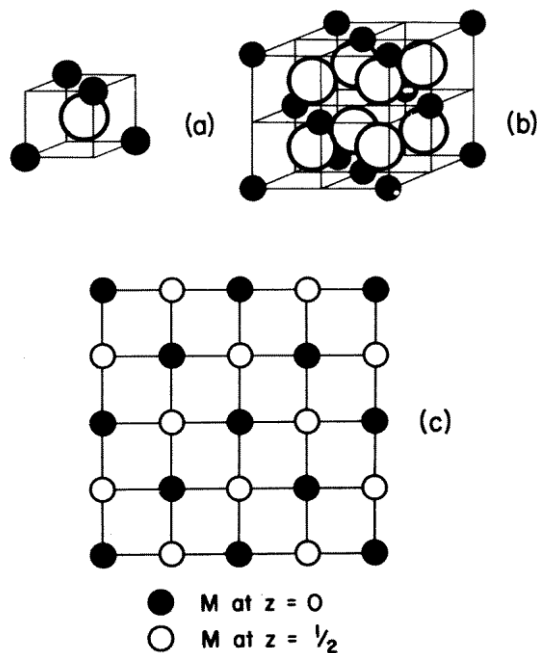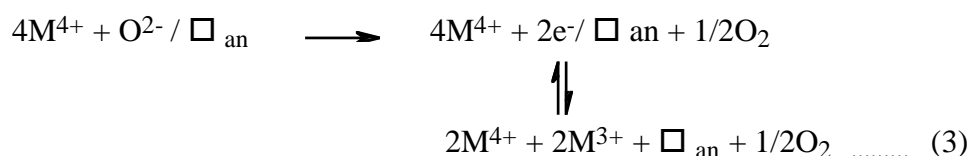
FIGURE 7.   Fluorite structure.   (a) octant of composition $M_{0.5}O$;
(b) unit cell (8 octants) of composition M_4O_8;   (c) matrix
representation for layer of 16 octants (composition M_8O_{16}).

generate the fluorite unit cell of composition M_4O_8 and edge length a_F.   A single layer of octants can be represented conveniently in projection by employing the square matrix illustrated in Fig. 7c with oxygen sites envisaged at the centre of each square.

Non-stoicheiometric oxides MO_x (*cf*. Table 2) with compositions in the range $1.5 \leq x \leq 2.0$ result from the removal of oxygen from octant centres leaving vacant anion sites according to the equation:

$$4M^{4+} + O^{2-} / \square_{an} \longrightarrow 4M^{4+} + 2e^{-}/ \square_{an} + 1/2O_2$$

$$2M^{4+} + 2M^{3+} + \square_{an} + 1/2O_2 \quad .... \quad (3)$$

where the symbol $\square_{an}$ denotes an anion site denuded of oxygen.   For binary oxides (CeO_x) imbalance between anionic and cationic charge is accommodated by changing proportions of the two oxidation states Ce^{3+} and Ce^{4+}.   Kinetic barriers to configurational rearrangements in binary oxides are small since inequalities of charge can be redistributed readily by electron transfer between metal cations.   On the other hand, electron hopping between aliovalent ions (*i.e.,* solute cations of different oxidation state from the corresponding solvent cation) in ternary oxides such as CaO/ZrO_2 is precluded and the activation energy to ordering processes may be considerable.   In these circumstances the distribution of aliovalent cations will pre-determine the location of the compensating defects in the anion sub-lattice.

The Coordination Defect: Topological Analysis

There are several single crystal X-ray structure determinations of fluorite type oxides which are of sufficient accuracy to confirm that every anion vacancy is circumscribed by the six nearest neighbouring oxygen atoms which are contracted inwards as though under the influence of a polarizing positive charge.   In other words, the point defect $\square$ appears
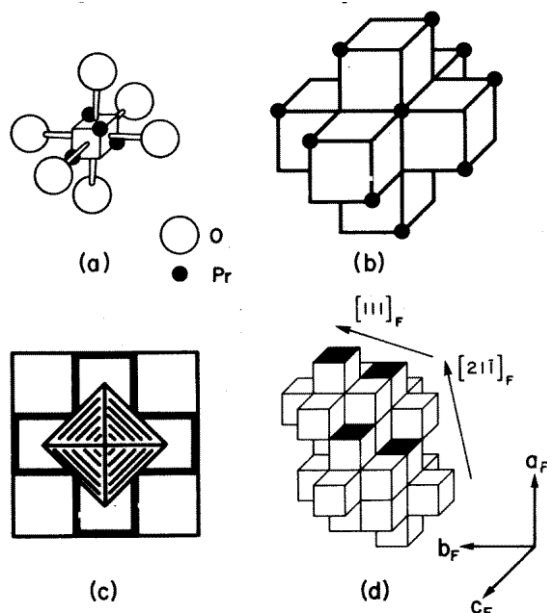

FIGURE 8. (a) Stereochemical environment of vacant anion site;   (b) topology of coordination defect with composition $M_{3.5}\square O_6$;   (c) octahedrally coordinated anion vacancy $\square O_6$ in projection on fluorite matrix;   (d) cluster of four c.d.s occurring in $\ulcorner$-Pr_7O_{12} showing important directions.

to have no independent existence but, in its coordinated state $\square O_6$ (Fig. 8a), becomes a structural entity which places effective limitations on the number of alternative ways in which a given anion deficiency can be accommodated by the parent lattice.   Furthermore, by employing our unconventional anion-centred reference frame, we can now depict a vacant anion site by the conventional projection of an octahedron along its four-fold symmetry axis (Fig. 8c).

Before proceeding to explore the structural role played by the coordinated vacancy, $\square O_6$, it is necessary to establish its topology and chemical composition.   Since the cation sub-lattice remains intact, the true coordination defect (c.d.) is comprised of the seven octants illustrated in Fig. 8b which circumscribe the anion vacancy and each of its six nearest O^{2-} neighbours.   The overall composition of the c.d. is $M_{3.5}\square O_6$ and its unique topology is consequent on the octahedral distribution of the six encapsulating octants.

In order to construct an oxide phase based on closest packing of c.d.s, they need to be aligned in rows parallel to the $[0\bar{2}1]_F$ direction (Fig. 9).   Two mating holes (H) per c.d. must be incorporated in each $(100)_F$ layer to enable the topological requirement of
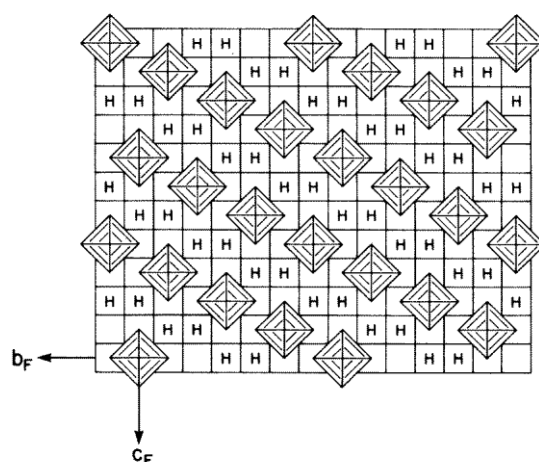
FIGURE 9. Idealized square-matrix representation of a $(100)_F$ layer of the fluorite lattice showing the location of vacant oxygen sites in Γ-Pr_7O_{12} along $[0\bar{2}1]_F$ and $[0\bar{1}\,\bar{3}]_F$ directions. Mating holes for accommodating contiguous layers are designated by H.

c.d.s in contiguous layers to be accommodated. The three-dimensional assembly of c.d.s is uniquely determined by their topology and since it is space filling (Fig. 8d), the overall composition of the phase is M_7O_{12} which corresponds to ~14% of untenanted anion sites.

A number of binary and ternary oxide phases with this composition are known (*e.g.,* Γ-Pr_7O_{12}, $Zr_3Sc_4O_{12}$, $Zr_3Yb_4O_{12}$, ULu_6O_{12} and UY_6O_{12}) and in each case their structure conforms with that deduced from the above topological considerations. Since each vacancy along $[0\,\bar{1}\,3]_F$ is related to another by the vector $\frac{1}{2}[21\bar{1}]_F$, they are gathered on oblique $(23\bar{1})_F$ planes and occur as metal-centred pairs in rows along the $[111]_F$ direction (Fig. 8d). The detailed nature of the superstructure emerges clearly if the vacant anion sites in a $(111)_F$ plane of the Γ-Pr_7O_{12} structure (Von Dreele *et al*., 1975) are delineated by their oxygen polyhedra (Fig. 10).
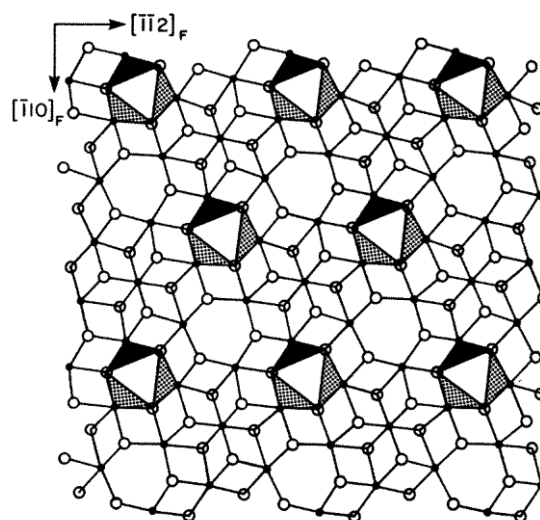

FIGURE 10. Section of Γ-Pr_7O_{12} structure perpendicular to $[111]_F$ axis. Arrangements of vacant anion sites in a $(111)_F$ layer is shown by their coordination octahedra.

Attempts to visualize the planar ordering of vacancies in terms of the metal-centred representation of Fig. 6 are less effective, the paired c.d. $M_7O_{12} \square_2$ having to be replaced by the much larger M_7O_{36} defect cluster (Thornber *et al.*, 1968) comprising the six MO_6 polyhedra (white cubes) which share edges with a central MO_6 polyhedron (black cube) which has a pair of vacant oxygen sites disposed across its [111] body diagonal (Fig. 11).
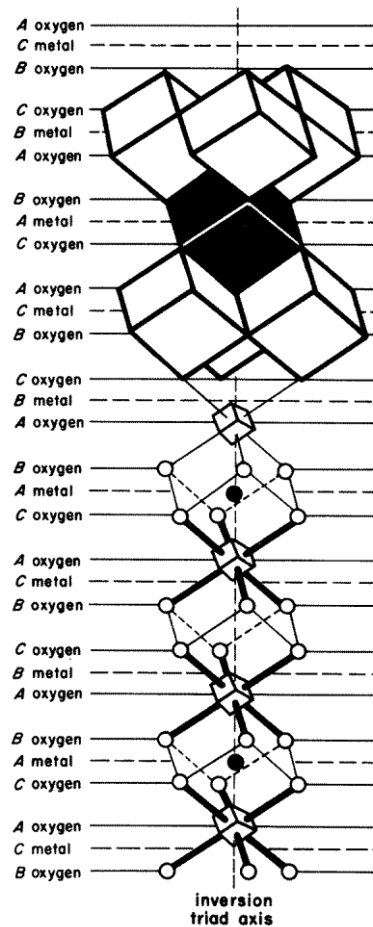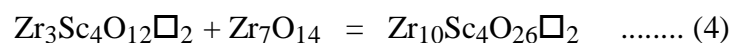

FIGURE 11. M_7O_{36} defect cluster and the octahedrally coordinated anion vacancies $\square O_6$ delineated along the same $[111]_F$ axis.

In addition to $Zr_3Sc_4O_{12}$, there is a second more oxidized but closely related phase, ©-$Zr_{10}Sc_4O_{26}$, which occurs in the ZrO_2-Sc_2O_3 system.   Once again, the vacant anion sites (7%) are ordered and structural features in common emerge when the distributions of coordination defects are viewed on an $(01\bar{1})_F$ plane (Fig. 12).   In both rhombohedral structures, the vacant anion sites lie along the $[111]_F$ direction occurring always as metal-centred pairs.   The difference in composition between the two phases is seen to arise from the periodic annihilation along $[111]_F$ of a pair of c.d.s by substitution of a pair of fluorite $Zr_{3.5}O_7$ entitites of identical topology which generates the composition of the ©-phase;
viz.,

$$Zr_3Sc_4O_{12}\square_2 + Zr_7O_{14} \ = \ Zr_{10}Sc_4O_{26}\square_2 \quad .... (4)$$
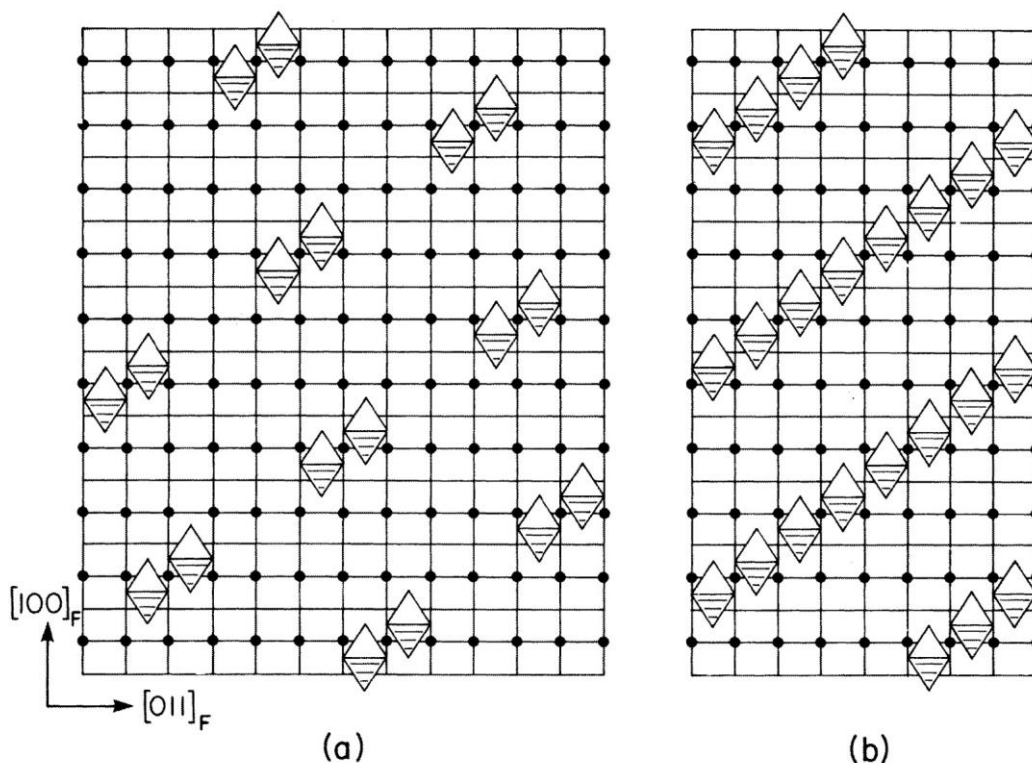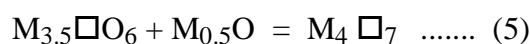
FIGURE 12.   Structure of (a) $Zr_{10}Sc_4O_{26}$ and   (b) $Zr_3Sc_4O_{12}$ shown on $(01\bar{1})_F$ planes.
Note metal-centred pairing of c.d.s along $[111]_F$ direction.

Ternary oxides of the pyrochlore type (naturally occurring mineral, $CaNaNb_2O_6F$) also have interesting electrical, magnetic and refractory properties.   This cubic M_4O_7 structure may be related to fluorite by deleting one-eighth of the anions in an ordered manner, the ternary oxides $La_2Ti_2O_7$ and $Gd_2Zr_2O_7$ providing examples (Table 2).   Alternatively the pyrochlore composition can be achieved by incorporating one fluorite octant ($M_{0.5}O$) per c.d. into the close-packed assembly which comprises the M_7O_{12} phase; *viz.*,

$$M_{3.5}\square O_6 + M_{0.5}O \ = \ M_4\,\square_7 \ .... \ (5)$$

It is generally found that the larger M^{3+} cation lies at the centre of a deformed MO_8-cube while the smaller M^{4+} cation occupies the centre of a $MO_6\square_2$ cube where the missing anions lie along a [111] body diagonal.   The resulting ordered arrangement of vacant anion sites in a $(100)_F$ layer is illustrated in terms of c.d.s in Fig. 13.

Homologous Series and Crystallographic Shear in Lanthanide Oxides

Several rare earth elements exhibit variable valency; in particular, cerium, praseodymium and terbium form both a tervalent and tetravalent sesquioxide M_2O_3 and dioxide MO_2.   In the intervening composition regions $MO_{1.5}$ - $MO_{2.0}$, the phase diagram (Fig. 14) reveals a rich variety of non-stoicheiometric phenomena (Hyde *et al.*, 1966).   At higher temperatures, non-stoicheiometric disordered phases of widely variable composition MO_x occur.   However, at lower temperatures a series of structurally ordered line phases

of quite narrow composition range develop. Their composition is well-defined conforming to the homologous series Pr_nO_{2n-2} with n = 6, 7, 9, 10, 11 and 12 (*cf.* Table 2).
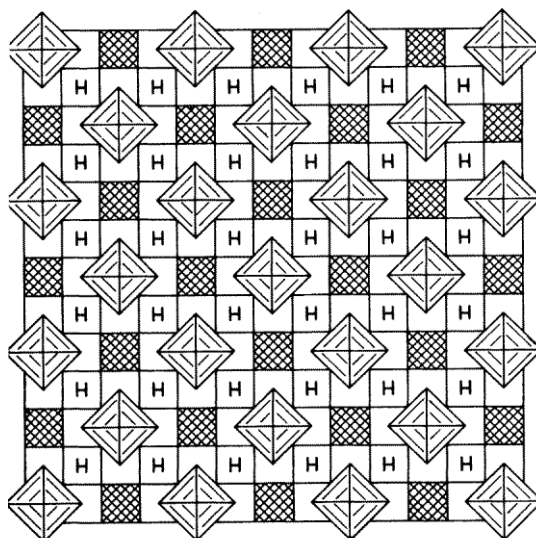

FIGURE 13. Pyrochlore structure M_8O_{14}. Idealized matrix representation of a $(100)_F$ layer showing location of vacant oxygen sites as c.d.s. Additional $M_{0.5}O$ octants are cross-hatched.

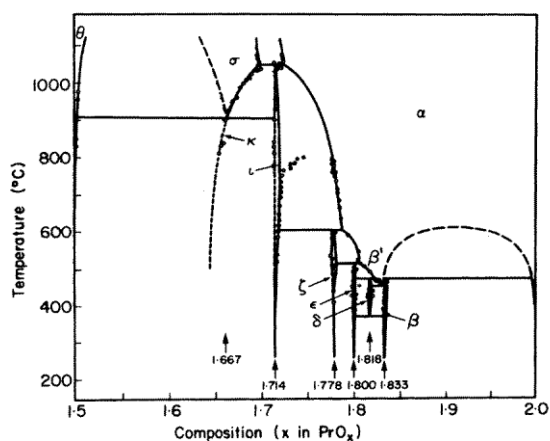FIGURE 14. Projection of the PrO_x ($1.5 \leq x \leq 2.0$) phase diagram on the temperature-composition plane. Compositions and designations of ordered phases are marked.

The detailed structural characterization of these intermediate phases has remained an elusive problem of significance in understanding the nature of fluorite related defect solids. Although the crystal structures are not known, the dimensions and symmetry of the superlattices have been obtained from high-resolution transmission electron microscopy of microcrystalline materials (Kunzmann *et al.*, 1975). When combined with the topological restrictions imposed by the c.d., model structures can be devised which possess edge dimensions and directions which bear identical relationships to the parent fluorite structure as do the *a*, *b* and *c* axes of the observed unit cells.
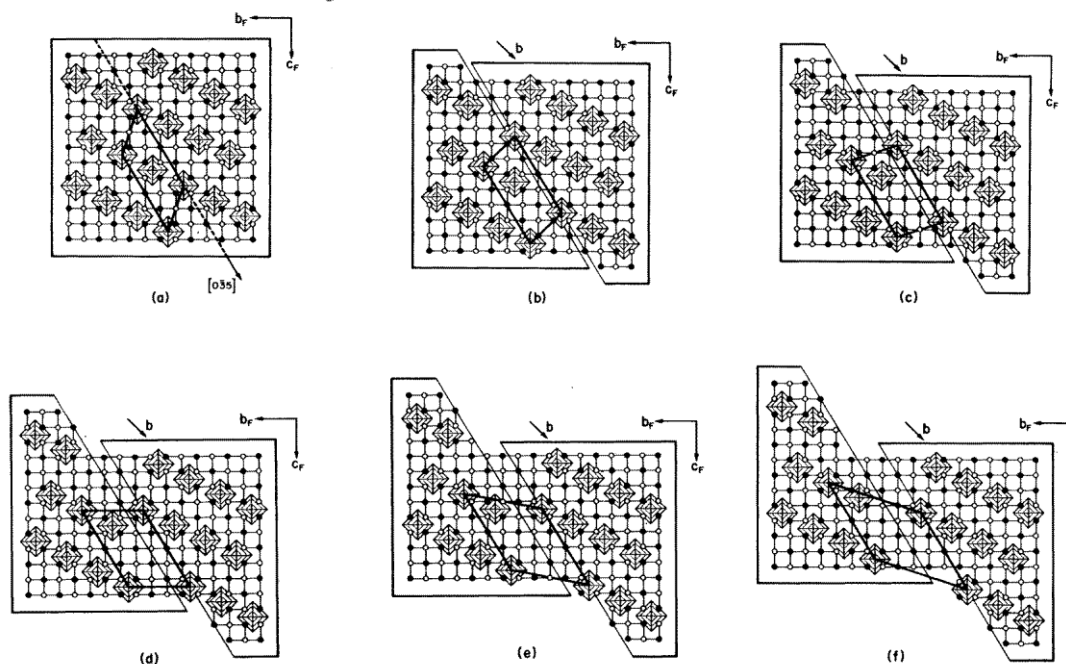
FIGURE 15. (a) an idealized $(100)_F$ structural octant layer of $\lceil$-Pr_7O_{12} showing the line in the $(0\bar{3}5)_F$ direction along which oxygen sites will be created using the shear operation $1/2(01\bar{1})_F$. The metal atoms can be regarded as invariant. (b) Formation of $(1\bar{5}3)/\!\!/ 2[\bar{0}11]_F$ shear plane corresponding to the production of a $(1\bar{5}3)_F$ sheet of composition Pr_8O_{14} inserted coherently into the parent $\lceil$-Pr_7O_{12} matrix (b = Burgers vector).
(c) The formation of a $(100)_F$ octant layer of the $\lceil$-Pr_9O_{16} phase by the incorporation of two additional $(1\bar{5}3)_F$ anion planes into $\lceil\square Pr_7O_{12}$ using the CS procedure above. (d) Conjectural triclinic modification of $Pr_{10}O_{18}$. (e) ^{TM}-$Pr_{11}O_{20}$; observed structural repeat unit outlined in black. (f) Conjectural triclinic modification of $Pr_{12}O_{22}$.

The existence of the Pr_nO_{2n-2} series derives from blending y octants of composition $Pr_{0.5}O$ with the c.d. progenitor $Pr_{3.5}\square O_6$ to yield the homologue $Pr_{(3.5+0.5y)}\square O_{(6+y)}$; i.e., Pr_nO_{2n-2} where n = $(y+7)$. This uniform progression suggests that the homologues might be inter-related, at least formally if not mechanistically, through a process of crystallographic shear (Hoskins *et al.*, 1976). The possibility of applying crystallographic shear to an oxygen-centred lattice is an advantage consequent on the persistence of the octahedral $\square O_6$ entity and the invariance of the f.c.c. metal lattice in the fluorite oxides. The crystallographic shear operation can be visualized conveniently by first cutting a drawing of a $(100)_F$ octant layer of $\lceil$-Pr_7O_{12} along the trace $[0\bar{3}5]_F$ of a $(1\bar{5}3)_F$ plane on $(100)_F$ (Fig. 15a). The $(100)_F$ layer is now opened up by shearing in the $[0\bar{1}1]_F$ direction to create new oxygen sites. For example, the CS operation $[0\bar{1}1]_F$ enables two additional $(1\bar{5}3)_F$ planes of PrO_2 (i.e., y = 2) to be inserted coherently into the parent $\lceil\square Pr_7O_{12}$ matrix corresponding to the formation of a sheet of $\lceil$-Pr_9O_{16} (Fig. 15c). Similarly, the model which reproduces the unit cell characteristics of the ^{TM}-$Pr_{11}O_{20}$ phase can be generated from $\lceil$-Pr_7O_{12} by the CS operation $2[011]_F$ as shown in Fig. 15e. In this case, four new $(153)_F$ planes of PrO_2 (*i.e.* y = 4) are introduced coherently into the $\lceil$-Pr_7O_{12} matrix to generate the composition $Pr_{11}O_{20}$.

The structural repeat units outlined in black in Fig. 15 can be stacked along a_F to give triclinic unit cells which reproduce the $1/2[21\bar{1}]_F$ and $1/2[\bar{1}\bar{1}2]_F$ vectors observed for the a and c axes of the super-structures respectively. Although the vacancies are grouped again as metal-centred pairs with a local $[111]_F$ axis, the pairs now lie along $[21\bar{1}]_F$ and $[1\bar{1}2]_F$ directions being gathered in $(1\bar{5}3)_F$ layers.

The CS operations $3/2[0\bar{1}1]_F$ and $5/2[0\bar{1}1]_F$ generate unknown triclinic polymorphs of the known monoclinic homologues Σ-$Pr_{10}O_{18}$ and ®-$Pr_{12}O_{22}$. This suggests that the structural relationships between the odd- and even-membered phases are likely to be close. This topic has been discussed further elsewhere (Hoskins *et al*., 1976).

Extended Defects: Corner and Edge-Sharing of Coordination Defects

The structures of $Zr_{10}Sc_4O_{26}$, pyrochlore and the Pr_nO_{2n-2} homologues are based on an ordered distribution of isolated coordination defects padded out with $M_{0.5}O$ fluorite octants. The most reduced fluorite-type structure based on the close-packing of isolated c.d.s is M_7O_{12}. Any further reduction inevitably leads to corner- and/or edge-sharing of c.d.s if the octahedral coordination about a vacancy is to be preserved (Hoskins *et al*., 1975). The structures of two ternary phases of composition $MO_{1.667}$ ($n = 6$) have been reported (*cf*. Table 2) and both conform with the topological expectations of the c.d. model. For example, the structure of monoclinic strontium uranate (Loopstra *et al*., 1969) involves strings of c.d.s along $[100]_F$ which are joined by sharing corners (Fig.16b). The ordered vacancies are contained on every fourth $(0\bar{1}1)_F$ plane which has the composition $[UO\square]^{4+}$ (*cf*., Fig. 16b). This ordered vacancy plane is sandwiched between

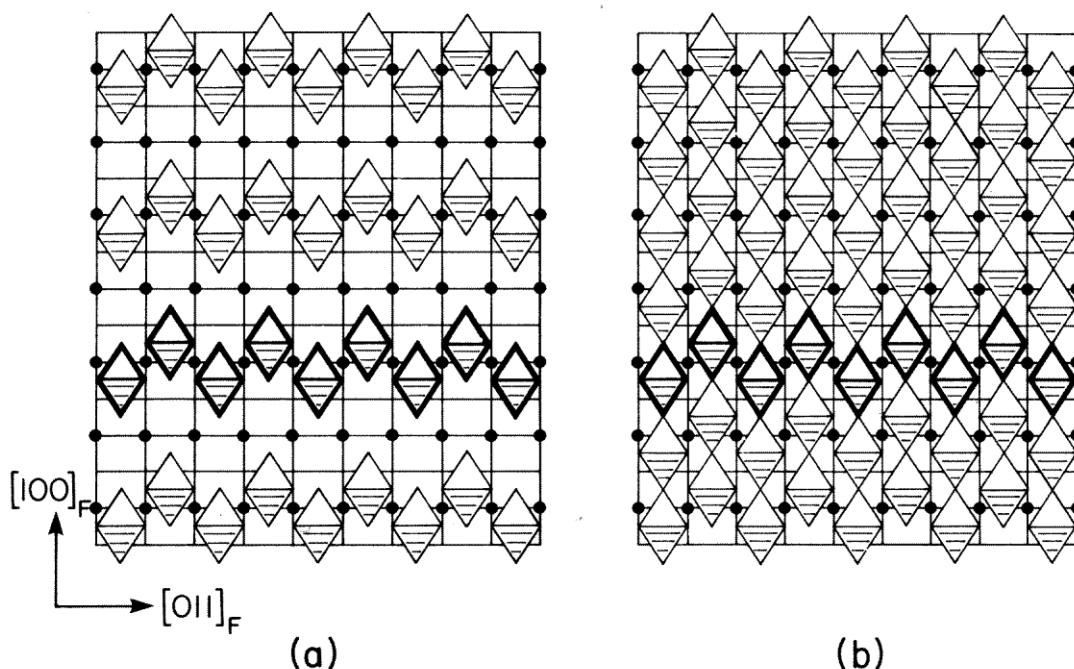FIGURE 16. Structure of (a) pyrochlore and (b) Sr_2UO_5 (or ®-Bi_2O_3) on an $(0\bar{1}1)_F$ plane. The rows of c.d.s along $[011]_F$ form "extended defects" (outlined), the anion vacancies being related by either $[111]_F$ or $[1\bar{1}\bar{1}]_F$ metal-centred vectors.

two $(01\bar{1})_F$ intact planes of $[SrO_2]^{2-}$ to complete the composition of the phase Sr_2UO_5. The structure of cadmium uranate (Sterns *et al*., 1964) is similar; the structure of |-Pr_6O_{10} is not known.

Although more reduced oxide phases corresponding to $n = 5$ have not been characterized, there are many examples of metal sesquioxides (*i.e.*, $n = 4$) with structures related to fluorite (*cf*., Table 2). Examination of the cubic structures of ®-Bi_2O_3 and type C-Ln_2O_3 (bixbyite or or ⟨-Mn_2O_3 type) has established that both are based on a f.c.c. metal lattice. Furthermore, in both structures, the 25% anions are omitted from fluorite sites in an ordered rather than a random manner. Each vacant oxygen site is surrounded by an octahedron of oxygen atoms so that the integrity of the c.d. remains preserved in these highly reduced phases.

In the cubic ®-Bi_2O_3 structure (Gattow *et al*., 1964) each c.d. shares all six apices with neighbouring c.d.s to achieve the desired $\Box O_3$ stoicheiometry (Fig. 17a). The resultant $\Box O_{6/2}$ infinite network is reminiscent of the metal-centred ReO_3 lattice (Fig. 5a) except that the oxygen vacancies lie at the rhenium atom sites (N.B. there are actually two interpenetrating ReO_3-like sub-lattices in ®-Bi_2O_3). If the cubic ®-Bi_2O_3 structure is viewed on $(\bar{0}1\,1\,)_F$ planes, the arrangement of vacant anion sites is identical to that found on $(01\,1\,)_F$ planes in Sr_2UO_5 (Fig. 16b). Each ordered vacancy plane of composition $[BiO\Box]^+$ alternates with an oxygen-intact $(01\bar{1})_F$ plane of composition $[BiO_2]^-$ to generate the sesquioxide composition and structure.

(a)

$\frac{1}{2}[00\bar{1}]_F$

$\frac{1}{2}[0\bar{1}0]_F$

(c)

(b)
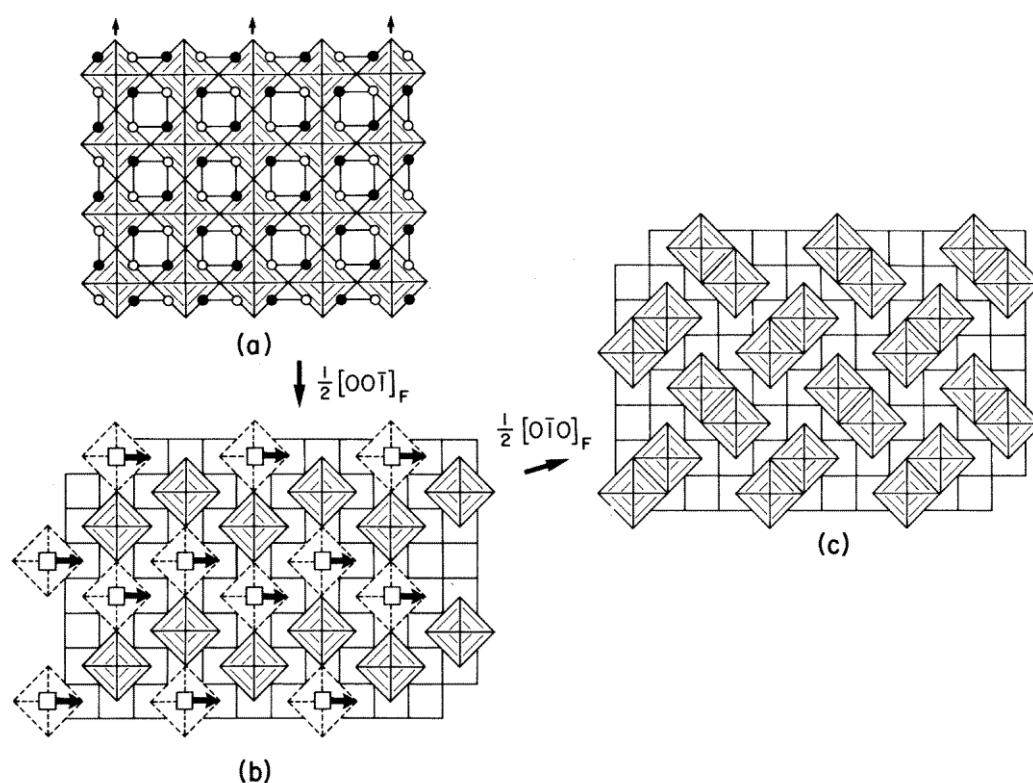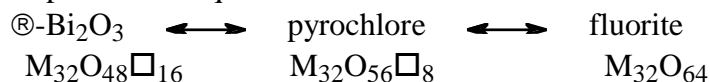
FIGURE 17. Transformation of ®-$Bi_2O_3 \longrightarrow$ type C-M_2O_3. (a) arrangement of c.d.s in $(100)_F$ layer of ®-Bi_2O_3 structure; (b) $(100)_F$ layer of type D-M_2O_3 generated by $c/2$ slip of alternate $[001]_F$ rows of c.d.s in direction arrowed in (a); (c) $(100)_F$ layer of type C-M_2O_3 derived from type D by the $b/2$ slip mechanism depicted in (b).

A close relationship between ®-Bi_2O_3 and the cubic pyrochlore phase M_4O_7 also emerges on $(01\bar{1})_F$. The vacancy-containing $(01\bar{1})_F$ plane in pyrochlore contains only one-half the density of vacant sites so that apex sharing between c.d.s is no longer involved (Fig. 16a). This plane of composition $M_2O_3\square$ alternates with an oxygen-intact plane M_2O_4 to generate the pyrochlore composition. The rows of c.d.s along $[011]_F$ form an "extended defect" with the anion vacancies being related either by $[111]_F$ or $[\bar{1}\bar{1}1]_F$ vectors. (This "extended defect" was originally termed a "duplex" row of c.d.s by Martin, 1974.) These "extended defects" are also a characteristic of Sr_2UO_5 except that corner-sharing between them occurs along $[100]_F$. These transformational relationships correspond to the compositional sequence:

$$\text{®-}Bi_2O_3 \longleftrightarrow \text{pyrochlore} \longleftrightarrow \text{fluorite}$$
$$M_{32}O_{48}\square_{16} \qquad M_{32}O_{56}\square_8 \qquad M_{32}O_{64}$$

The type C-M_2O_3 bears a different relationship to the fluorite structure. It also involves the regular omission of one-quarter of the oxygen atoms, a small distortion of the metal lattice from f.c.c., and a unit cell of b.c.c. symmetry with double the fluorite edge (Paton *et al*., 1965). Again, every vacant anion site is coordinated by an octahedron of nearest oxygen neighbours to yield an ordered vacancy superstructure based on c.d.s. However, unlike ®-Bi_2O_3, each $\square_6$ octahedron shares three of its edges with three $\square O_6$ nearest neighbours to achieve the desired stoicheiometry $\square O_3$. These neighbours, and hence the edges involved, are related by a three-fold symmetry axis passing through the centrally coordinated c.d., all four c.d.'s being situated on the

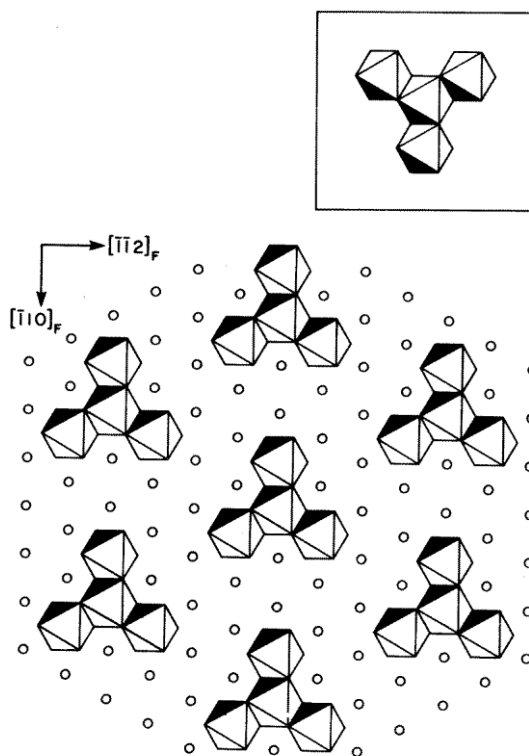FIGURE 18. Type C-M_2O_3. Arrangement of vacant anion sites on a $(111)_F$ plane showing their coordination octahedra. The ⊄ chirality of the ©-shaped clusters in this plane is contrasted with the Δ configuration of adjoining $(111)_F$ planes shown in the inset.

same $(111)_F$ plane.   Effectively, each c.d. is "tris-chelated" by its three neighbouring c.d.s conferring on it the property of chirality, i.e., Δ and $\not\subset$ configurations occur in equal proportions in the structure (Hoskins *et al.,* 1975).   The arrangement of vacancies on a $(111)_F$ plane is depicted in Fig. 18.

The chiral properties of each $(111)_F$ layer determine the manner in which the Y-shaped clusters link up with their neighbours in next-nearest, rather than nearest, layers.   Two interpenetrating, but unconnected networks of c.d.s, each of opposite chirality, are generated throughout the type C-M_2O_3 structure, one involving the layers numbered 1,3,5 etc. ($\not\subset$ chirality; Fig. 18) and the other 2,4,6 etc. ($\otimes$ chirality).   The $\not\subset$ network which results from edge-sharing of c.d.s between layers 1,3 and 5 is illustrated in projection on $(111)_F$ in Fig. 19.   Layer 7 exactly overlays layer 1 of this diagram, the pattern repeating itself throughout the lattice.   The corresponding projection of the even-numbered layers, *i.e.,* those of opposite chirality, intermeshes perfectly so that the lacunae of the projection shown in Fig. 19 disappear.
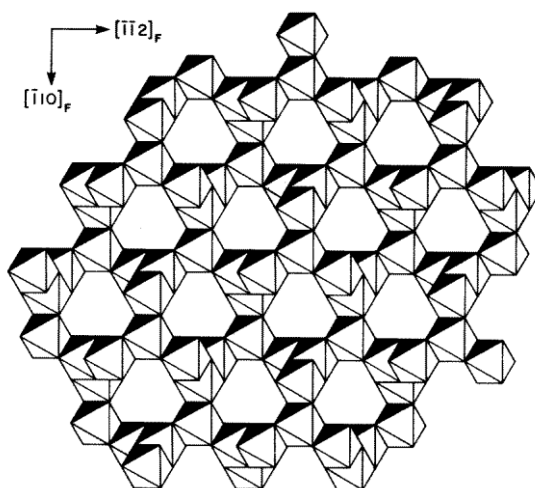

FIGURE 19.   Type C-M_2O_3.   One of the two interpenetrating networks of c.d.s ($\not\subset$ chirality) showing the edge-sharing involved between planes 1, 3 and 5.

The edge-sharing between c.d.s within each single $(100)_F$ layer of the type C structure (Fig. 17c) produces a pattern of isolated "pairs" which differs distinctively from the apex-sharing linkages of c.d.s which characterize the ®-Bi_2O_3 structure (Fig.17a). However, the relationship between the two structures is extremely close and the transformation

$$®\text{-}Bi_2O_3 \quad \longleftrightarrow \quad \text{type C-}M_2O_3$$

can be effected by a series of concerted oxygen/ vacancy exchanges over minimal distances (of either $a/2$ or $a\sqrt{2}$); viz.,

$$O^{2-} + \square \quad \rightleftharpoons \quad \square + O^{2-} \quad ....(6)$$

This transformation is illustrated schematically for the single $(100)_F$ oxygen plane in Fig. 17a.   The first step involves the translation by $a/2$ of every alternate $[011]_F$ string of apex-sharing c.d.s to give the precursor shown in Fig. 17b. This translation operation

$1/2[01\bar{1}]_F$ is similar to introducing an antiphase boundary (a.p.b.) by crystallographic shear, the composition M_2O_3 remaining unchanged by the CS operation. The precursor structure differs, however, from ®-Bi_2O_3 and C-M_2O_3 in that it is based on a combination of apex-sharing c.d.s in *trans*-$[001]_F$ positions and edge-sharing of c.d.s in the $[\bar{1}10]_F$ direction. (This conjectural phase has not been observed experimentally and for convenience is referred to as type D-M_2O_3.) The second translation operation $1/2[\bar{0}10]$ illustrated in Fig. 17b is also a.p.b. in nature and generates a $(100)_F$ plane of unchanged composition with the type C-M_2O_3 structure (Fig. 17c).

Unlike the ®-Bi_2O_3 and pyrochlore structures, two types of vacancy plane, A and B, occur on $(01\bar{1})_F$, for type C, there being no oxygen intact planes. These are represented in Fig. 20,
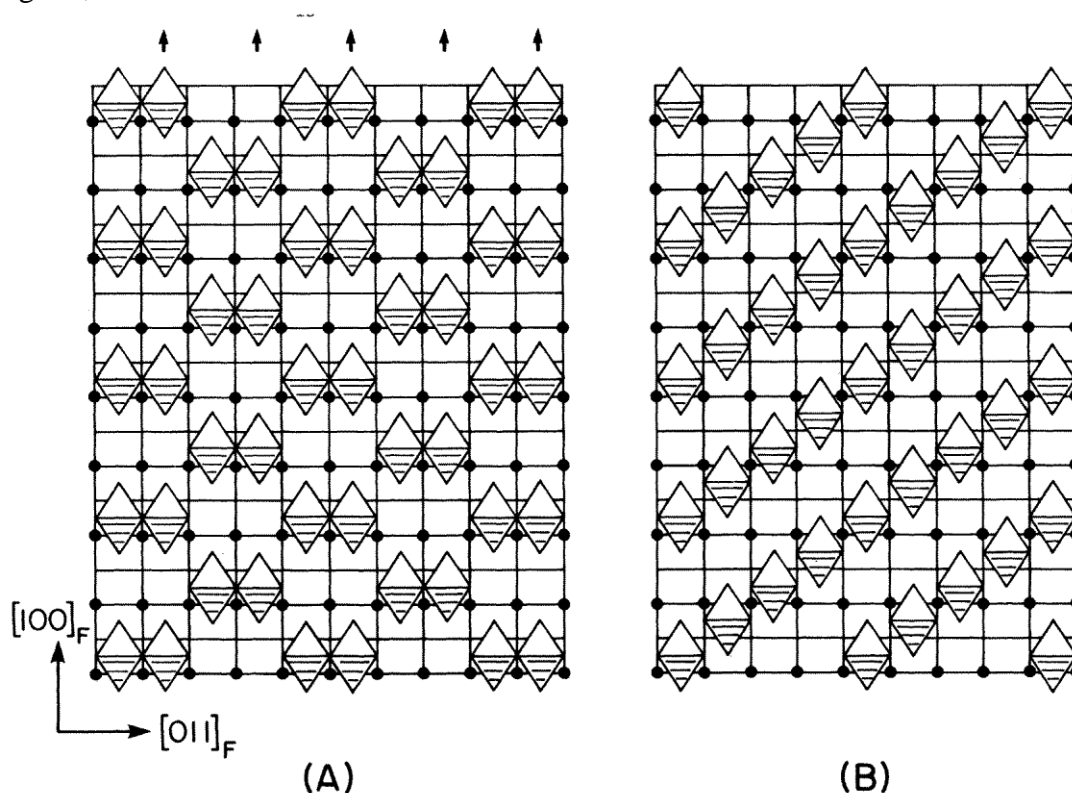

FIGURE 20. Type C-M_2O_3. Two $(01\bar{1})_F$ planes, denoted A and B, which alternate in the structure. Plane A is converted to plane B by *a*/2 slip of alternate $[100]_F$ rows of c.d.s in the direction of the arrows.

both A and B having the same composition $M_4O_6 \square_2$. A and B planes alternate throughout the type C structure generating the two interpenetrating sub-lattices of Δ and $\not\subset$ chirality (*cf*., Fig. 18). Metal-centred pairing of c.d.s along $[111]_F$ is evident in the B planes. An interesting feature of this beautifully ordered structure is that the sub-lattices of
Δ and $\not\subset$ chirality can be regarded as two independent giant extended defects which nevertheless are "paired" along $<111>_F$ by six-coordinated metal atoms at the $\Delta/\not\subset$ interfaces.

Conclusions

Our concept of the real structure of a non-stoicheiometric solid has changed dramatically during the past 10-15 years. The classical idea of a random distribution of

point defects has become unacceptable as a basis for explaining gross departures from simple stoicheiometry. Point defects in non-stoicheiometric oxide phases with either the rock salt or the fluorite structure undergo aggregation to more complex structural units which tend to be distributed throughout the host lattice in a regular periodic fashion. These may be discrete clusters or extended defects in two or three dimensions. This tendency to order when carried to completion generates a super-lattice of the parent compound which for specific cation/anion ratios frequently defines a homologous series. The "cluster" and the "extended defect" become an integral component of the superstructural pattern, so much so that it can be argued that the ordered non-stoicheiometric phase is a new structure in its own right.

Recognition of the topology of the coordinated point defect enables common features of related crystal structures to be identified and their structural transformations to be better understood. This is especially important for materials such as oxides of the fluorite type where location of missing oxygen atoms by direct methods is inherently a formidable experimental task. Topological analysis of defect fluorite phases has wider implications of significance for other areas such as the magneto-optical properties of crystalline solids. For example, the green fluorescence of CaF_2 when doped with small amounts of uranium is observed only in the presence of oxygen and so has been attributed to U^{6+} coordinated by oxygen ligands. The polarized Zeeman spectra, which differ in character from those of uranyl (UO_2^{2+}) compounds, establish that the electronic transition occurs at a centre with trigonal and inversion symmetry (Manson *et al.*, 1975). These restrictions can be satisfied if the emitting centre is comprised of a metal-centred pair of c.d.s of composition $UCa_6O_6F_6\square_2$ (*i.e.*, M_7O_{12} type) intergrown coherently in the host CaF_2 lattice (Fig. 21).
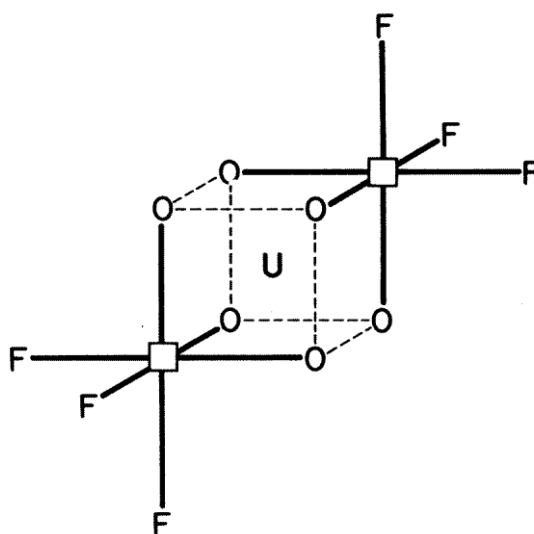

FIGURE 21. Conjectural structure of the emitting centre responsible for green fluorescence of fluorite doped with small amounts of uranium (VI). The uranium(VI) centred pair of c.d.s has the overall composition $UCa_6O_6F_6\square_2$.

The growing demand for new materials in high temperature and electronic technology will ensure that the complex inter-relationships between composition, structure and properties, which form the basis of research into the defect solid state, will remain a vital field of chemical endeavour.

Acknowledgment

I am indebted to my colleagues, Dr. B.F. Hoskins and Dr. D. Taylor for many stimulating discussions.

References

Allpress, J.G., 1969. *J. Solid State Chem.,* **1**, 66.

Allpress, J.G., Sanders, J.V., and Wadsley, A.D., 1969. *Acta Cryst.,* **B25**, 1156.

Anderson, J.S., 1974. *Defects and Transport in Oxides* (Eds. M.S. Seltzer, and R.I. Jaffee). Plenum Press. pp. 25-48.

Anderson, J.S., and Hyde, B.G., 1967. *J. Phys. and Chem. Solids,* **28**, 1393.

Bursill, L.A., and Hyde, B.G., 1970. *Phil. Mag.,* **23**, 3.

Gattow, G., and Schütze, H. A 1964. *Z. anorg. Chem.,* **328**, 44.

Hoskins, B.F., and Martin, R.L., 1975. *J. Chem. Soc. (Dalton)*, 576.

Hoskins, B.F., and Martin, R.L., 1976. *J. Chem. Soc. (Dalton),* 676.

Hyde, B.G., Bevan, D.J.M., and Eyring, L., 1966. *Phil. Trans. Roy. Soc., (London),* **A259**, 583.

Koch, F., and Cohen, J.B., 1969. *Acta Cryst.,* **B25**, 275.

Koyama, H., and Saito, Y., 1954. *Bull. Chem. Soc. Japan,* **27**, 112.

Kunzmann, P., and Eyring, L., 1975. *J. Solid State Chem.,* **14**, 229.

Loopstra, B.P., and Rietveld, H.M., 1969. *Acta Cryst.,* **B25**(4), 787.

Manson, N.B., Shah, G.A., and Runciman, W.A., 1975. *Solid State Commun.,* **16**, 645.

Martin, R.L., 1974. *J. Chem. Soc.(Dalton),* 1335.

Paton, M.G., and Maslen, E.N., 1965. *Acta Cryst.,* **19**, 307.

Sawyer, J.O., Hyde, B.G., and Eyring, L., 1965. *Bull. Soc. chim. France,* 1190.

Schottky, W., and Wagner, C., 1930. *Z. physik. Chem.,* **B11**, 163.

Sterns, M., and Sawyer, J.O., 1964. *J. Inorg. Nuclear Chem.,* **26**, 2291.

Thornber, M.R., and Bevan, D.J.M., 1970. *J. Solid State Chem.,* **1**, 536,

Thornber, M.R., Bevan, D.J.M., and Graham, J., 1968. *Acta Cryst.,* **B24**, 1183.,

Von Dreele, R.B., Eyring, L., Bowman, A.L., and Yarnell, J.L., 1975. *Acta Cryst.,* **B31**, 971.

Watanabe, D., Terasaki, O, Jostsons, A., and Castles, J.R., 1970. *The Chemistry of Extended Defects in Non-Metalic Solids.* (Eds. L. Eyring, and M. O'Keeffe.) North-Holland Publishing Co., pp. 238-258.